Nanofiltration performances after membrane bioreactor for hospital wastewater treatment: Fouling mechanisms and the quantitative link between stable fluxes and the water matrix

Yandi Lan, Karine Groenen-Serrano, Clémence Coetsier, Christel Causserand

Nanofiltration performances after membrane bioreactor for hospital wastewater treatment: Fouling mechanisms and the quantitative link between stable fluxes and the water matrix

Yandi Lan, Karine Groenen-Serrano, Clémence Coetsier, Christel Causserand*

Laboratoire de Génie Chimique, Université de Toulouse, CNRS, INPT, UPS, Toulouse, France

A B S T R A C T

Treatment combining membrane bioreactors (MBR) and nanofiltration (NF) is becoming an emerging wastewater treatment strategy. The combined process is capable of producing high quality water potentially reusable; however, diverse compositions of MBR effluents induce several types and degrees of NF membrane fouling that impacts process productivity. Moreover, since MBR effluent composition for one type of wastewater source is variable depending on the MBR efficiency at different periods, downstream NF membrane fouling types and degrees may consequently change over time.

In that context, the present paper aims at developing effective fouling control strategies of NF membrane in the case of the filtration of MBR effluents taken from a MBR system installed in a French hospital. These effluents were filtrated under various transmembrane pressures, and stable fluxes during these filtrations were determined. Several types and degrees of fouling mechanisms were then identified through surface morphology observation and the analysis of chemical compositions of fouled mem branes. The diverse flux behaviour was further associated with the fouling mechanisms and foulant compositions. Based on the study of these mechanisms, the quantitative link between stable fluxes and calcium phosphate concentrations in MBR effluents has been established.

1. Introduction

Fresh water scarcity and environmental sustainability require the development of effective wastewater treatment and reuse processes. Within this framework, membrane bioreactor (MBR) system, one of the attractive options, is increasingly applied in municipal and industrial wastewater treatment, due to many ad vantages, such as a higher organics' removal capability and less space requirements in comparison to conventional activated sludge (CAS) treatment (Judd, 2016; Xiao et al., 2014). These advantages of MBR are particularly relevant for treating wastewater from hospital (Beier et al., 2011; Kovalova et al., 2012; Pauwels et al., 2006). Moreover, combining MBR treatment with further purification processes, such as nanofiltration (NF) or reverse osmosis (RO) is becoming an emerging strategy for advanced treatment of hospital wastewaters at source before their discharge in municipal sewage system (Monnot et al., 2017). In that case, the objective of the NF/RO combined to MBR is to avoid the dilution of highly concentrated hospital wastewaters, in terms of toxic organic compounds, into the domestic wastewater (McArdell and Moser, 2010). MBR system enables the removal of major parts of organic matter and biode gradable compounds due to the biological reaction. This system also enables the efficient separation of biological sludge and turbidity due to the micro or ultrafiltration membranes installed in the system. The downstream NF process is capable of removing biorefractory micropollutants, hardness salts and heavy metals and therefore improving the water quality. Even if in certain conditions a reuse standard can be reached by NF permeate (Alturki et al., 2010; Wang et al., 2015), it is important to consider that NF would not allow complete rejection of salts, thus we could expect that the concentration of salts in the treated water will be too important to allow direct reuse without further treatment (Shanmuganathan et al., 2015). RO could alleviate this problem but dissolved organic matters present in the secondary effluent would not allow the direct use of RO filtration at this step of the combined process (Tang et al., 2016).

Nevertheless, NF membrane fouling remains a challenging issue for the sustainability of the combined process. Colloidal sized

substances and soluble inorganic compounds that are scarcely removed in MBR are the foulants of greatest concern for nano filtration (Schafer et al., 2005). The deposition of these foulants on NF membrane leads to a decline in process productivity and may even cause irreversible damage to membranes. It was previously shown that scaling by calcium phosphate is a major issue in tertiary treatment of wastewater using nanofiltration or reverse osmosis, due to high rejection of divalent ions and concentration polariza tion (Antony et al., 2011; Greenberg et al., 2005; Levchenko and Freger, 2016; Rathinam et al., 2018). Moreover, it was found that low TMP limits the retention of phosphorus using NF membranes in the case of acidic pH effluents (Schütte et al., 2015).

Furthermore, the complexity and variability of the composition of MBR effluents make it difficult to manage stable fluxes and control NF fouling. MBR effluents contain numerous salts, in addi tion to organic matter that may cause different types and degrees of membrane fouling. Studies in synthetic and real wastewater ma trixes have indicated that the composition and morphology of the foulant layer lead to diverse impacts on flux behaviour (Li and Elimelech, 2006; Contreras et al., 2009; Jacob et al., 2010). For example, stable fluxes for membranes fouled by humic acid and dextran exceed the fluxes obtained on membranes suffering from alginate fouling when foulant feed concentrations are the same (Contreras et al., 2009). Another study shows that the combination of organic and silica colloidal fouling induces a decrease in flux (flux decline 40 L/h.m^2) that is more significant than the simple sum of the flux declines. Decrease in flux was 10 L/h.m^2 for simple organic fouling and 20 L/h.m^2 for simple colloidal fouling (Li and Elimelech, 2006). Dissimilar flux behaviour has been reported during filtra tions of two types of MBR effluents that mainly differ in term of organic matter concentration and electrical conductivity. The total organic carbon concentration and the electrical conductivity of MBR effluent 1 were 8 mg L^{-1} and 894 μS cm^{-1} respectively, and those of MBR effluent 2 6 mg L^{-1} and 631 μS cm^{-1}. Flux dramati cally decreased to 20% of the initial flux for the MBR effluent 1, while the flux remained greater than 80% of the initial flux in MBR effluent 2 matrix (Jacob et al., 2010).

In addition, the MBR system efficiency depends on the operating conditions, such as hydraulic residence time and pH, in such a way these parameters, together with the composition of MBR influent wastewater, strongly affect the MBR effluent compositions (Onesios et al., 2009; Pauwels et al., 2006).

Beside several strategies to minimise NF fouling found in the literature (Hashlamon et al., 2016; Mohammad et al., 2015) which were recently reviewed (Meng et al., 2017), our previous study (Lan et al., 2017) has investigated a fouling control strategy by permeate flux optimization for further purification of MBR effluents using NF. The concepts of critical flux and limiting flux were applied. Briefly, critical flux is the flux below which a decline of flux over time, due to irreversible fouling, does not occur; above this critical flux irre versible fouling is observed (Bacchin et al., 2006). The limiting flux represents the maximum stationary permeate flux, which can be reached by increasing the transmembrane pressure with a given solution or suspension (Aimar and Field, 1992; Bacchin et al., 2006). Through an experimental study including the application of a range of transmembrane pressures, the measurement of the stable flux for each pressure, identification of the fouling mechanisms on the fouled membrane, and then theoretical investigations, it has been possible to:

1) estimate the critical flux for irreversibility and find that no measurable fouling took place under this flux value;
2) demonstrate that different fouling stages occurred when filtra tions were conducted above the critical flux. For low pressure ranges, before reaching the limiting flux, the stable flux tends to the value of the critical flux. In these conditions limited fouling occurs, solely involving the accumulation of silica and colloidal organics. For higher pressure ranges, a limiting flux whose value was lower than that of the critical flux was ob tained. The low stable flux was linked to a severe fouling, combining the effect of colloidal silica and organics fouling, and calcium phosphate scaling;
3) develop a method, which can correlate flux behaviour and fouling mechanisms, define and calculate a permeability before scaling (L_s). With the initial membrane permeability and the estimated value of L_s, a working diagram showing the flux behaviour versus the operating pressure was proposed. This diagram defines three separated regions: a non fouling region A, an organics fouling region B and a scaling region C. Fig. 1 in supplementary information's section shows these three regions and the experimental value of fluxes as a function of trans membrane pressure obtained during successive filtrations using the same MBR effluent as feed.

The present study deals with the treatment of real hospital wastewaters, known for its toxicity, complexity and variability, by the combination of MBR and NF processes. The aim of this work is to identify the key characteristics of MBR effluents that control fouling and flux decline, and to further establish a quantitative link between MBR effluent compositions (e.g. salt) and stabilized fluxes in NF filtration, for further purification of MBR effluents. In order to take into account the complexity and the variability of real MBR effluents, we sampled MBR effluents at different times of the day over a period of 145 days from a MBR system installed at Purpan hospital, located in Toulouse, France. The stable fluxes were observed during cross flow NF of these various real MBR effluents, and then analysed using the NF working diagram obtained in the previous study. The corresponding fouling mechanisms were investigated through morphology observation and chemical com positions analysis on fouled membrane surface and then correlated to stable flux behaviour. Finally, a quantitative link between MBR component concentrations and stable fluxes was proposed.

2. Theory

Concentration polarization is known as the process of accu mulation of retained solutes in the membrane boundary layer due to membrane selectivity towards various compounds (Sherwood et al., 1965). The effect of polarization concentration can be expressed using CP the concentration polarization degree:

$$CP \quad \frac{C_m}{C_b} \tag{1}$$

where C_m and C_b are the solute concentration at the membrane surface and in the bulk, respectively.

The concentration polarization is reversible, whilst contributing to the development of problematic fouling, such as adsorption, gel layer formation and precipitation of solutes (Sablani et al., 2001).

Based on the boundary layer mass balance, the stable permeate flux J_{stab} (m s^{-1}) in the presence of polarization concentration, can be described by the Film Theory (Staff, 2011).

$$J_{stab} \quad \frac{D}{\delta} \ln\left(\frac{C_m \quad C_p}{C_b \quad C_p}\right) \quad k \ln\left(\frac{C_m \quad C_p}{C_b \quad C_p}\right) \tag{2}$$

where D (m^2 s^{-1}) and δ (m) are the solute diffusivity and the boundary layer thickness, respectively, k is the solute mass transfer coefficient (m s^{-1}) and C_p the permeate solute concentration.

Membrane scaling (or inorganic fouling) results from the

concentration of one or more species beyond their solubility limits and their precipitation onto the membrane surface (Antony et al., 2011). The precipitation of inorganics on a membrane surface re lates to the supersaturation rate, which is the thermodynamic driving force for precipitation. Considering an ionic substance M_xN_y, the simplified supersaturation ratio in the bulk S is defined by (Schafer et al., 2005):

$$S \quad \frac{C_{M^{y+},b}\, C_{N^{x}\ ,b}}{K_{sp}} \tag{3}$$

where K_{sp} is the thermodynamic solubility product, $C_{M^{y+},b}$ and $C_{N^{x}\ ,b}$ are the ionic concentrations. For S > 1, the transition to solid is probable.

Indeed, precipitation of inorganics on membrane surface is actually related to the supersaturation ratio on the membrane surface (S_m) which can be described by Eq. (4):

$$S_m \quad \frac{C_{M^{y+},m}\, C_{N^{x}\ ,m}}{K_{sp}} \tag{4}$$

where $C_{M^{y+},m}$ and $C_{N^{x}\ ,m}$ are the ionic concentrations on the membrane surface. They are related to the bulk concentrations $C_{M^{y+},b}$ and $C_{N^{x}\ ,b}$, according to the concentration polarization degree CP as Eq. (1). So, the supersaturation ratio of inorganic scalants on membrane surface S_m can be written as:

$$S_m \quad \frac{C_{M^{y+},b}\, C_{N^{x}\ ,b}\, CP_{M^{y+}}\, CP_{N^{x}}}{K_{sp}} \tag{5}$$

In the present matrix, calcium and phosphate are potential scalants as we reported in the previous study (Lan et al., 2017). Calcium phosphate accumulation and scaling at membrane surface were previously studied on RO and NF mimetic surfaces that give some insight into mechanisms that govern the accumulation of these scalants in wastewater treatment by RO and NF processes (Rathinam et al., 2018).

The protonated species of phosphate relates to the pH of water. The fraction of phosphate for different pH levels is presented in Fig. 2 in supplementary information section.

The MBR effluent pH is in the range of 6–8; the phosphate is then in the form of a dihydrogen phosphate ion ($H_2PO_4^-$) or a hydrogen phosphate ion (HPO_4^{2-}) depending on the pH. The acidic dissociation constant of them is equal to 7.21.

$$H_2PO_4^- \rightleftharpoons HPO_4^{2-} + H^+ \qquad pK_a \quad 7.21 \tag{6}$$

These two ions enable the precipitation of various species. Table 1 in supplementary information section lists the solubility product of different species of calcium phosphate, where the phosphate is in the form of $H_2PO_4^-$ and HPO_4^{2-}.

3. Materials and methods

3.1. Feed water matrix

The NF feed (MBR effluent) comes from a MBR system installed at Purpan, a hospital located in Toulouse, France. This MBR system is an experimental pilot with a biological tank of 500 L operated with an effective sludge retention time of 40 days and a hydraulic residence time of 24 h. MBR was directly fed from the hospital's sanitary collection system and used immersed hollow fibre mem branes (polysulfone 0.2 μm, reference: UFWW50 IMMEM, Poly mem) developing a surface of 7 m^2.

In order to investigate the impact of MBR effluent compositions on NF flux and fouling behaviour we sampled MBR effluents at different times of the day for 145 days. This real effluent contains salts, organic matter and around 50 pharmaceuticals from 10 different therapeutic classes. The composition of this MBR effluent varied slightly over the investigated period, depending on oper ating conditions in the MBR process and on composition and vol ume of MBR influents which were affected by hospital activities (Quesada et al., 2015). This MBR system exhibited satisfactory pu rification performances in term of COD removal (75–95%), a removal of total nitrogen ranging from 6 to 62% due to adjustments of operating conditions over the campaign duration, and a low removal of phosphorus, which would require a specific treatment.

The range of characteristics of MBR effluents sampled for the present study are listed in Table 1 (these data are presented in details for each individual run in Table 2 in supplementary infor mation section); all these values were obtained using the analytical methods described in section 3.3.1.

All the effluents of the combined system were discharged in the municipal sewage system, which is currently the destination of all wastewaters of the hospital.

3.2. Membrane and nanofiltration apparatus

The membranes and NF set up have been presented in a pre vious publication (Lan et al., 2017). In brief, a NE 70 polyamide composite nanofiltration membrane (provided by Woongjin Chemical Co., Ltd.) was examined in this study. The cross flow nanofiltration unit is shown in Fig. 3 in supplementary informa tion section. The volume of the feed tank (1) is 10 L. The flat feet membrane (1.4×10^{-2} m^2) was installed into a Sepa CF II cross flow filtration cell (3). Permeate was collected in a vessel and weighed by a balance (5) connected to a computer for flux calculation.

After membrane compaction, filtrations were conducted at constant transmembrane pressures (5–35 bar) with a 0.3 m s^{-1} cross flow velocity. The operating pressures are presented in Table 2 in which A, B, C, D, E, F, G, H, I, K, L, M, P and Q are the serial names of the experiments. For each filtration, a new membrane sample and a new MBR effluent (collected at different periods) were used.

In order to simulate a feed and bleed continuous mode at a Volume Reduction Factor (VRF) of 5, the filtrations were conducted in two steps: firstly, in a concentration mode and secondly in a recirculation mode. This VRF of 5, corresponding to a recovery rate of 80%, is within the range that would be applied in a full scale system (30–90%) (DiGiano et al., 2000). The permeate flux was monitored during both filtration steps. In the concentration mode, the retentate stream was recycled into the feed vessel while the permeate was collected in the permeate tank. This mode corre sponds to a transient state as the retentate concentration increased with filtration time. After the VRF reached 5, both retentate and

Table 1
Characteristics of MBR effluents sampled from the MBR system installed at the hospital.

Items	Range value	Ions concentration (mg L ^{1})	Range value
pH	6.05 7.95	Na^+	34.04 222.40
COD mg L ^{1}	16.0 73.0	K^+	12.91 25.58
TOC mg L ^{1}	8.40 31.40	Mg^{2+}	2.74 5.07
HCO3-/CO32-	0.52 71.16	Ca2+	24.80 63.50
UV_{254}	0.30 0.84	Cl	36.12 64.99
		NO_3	7.10 217.65
		SO_4^{2}	15.95 209.60
		PO_4^{3} [a]	5.75 29.40

[a] Due to the analysis method, all the H_3PO_4, H_2PO_4 ^{1}, HPO_4^{2} and PO_4^{3} present in the solution were referred to as the PO_4^{3} form.

Table 2
Operating transmembrane pressures used during independent filtrations.

TMP (bar)	3	5	10	15	25	35
Filtration serials	M	I, H	K	E,G,F, L	A,B,N,P,Q	C,D

permeate streams were recycled back to the feed tank, corre sponding to a recirculation mode.

Membrane initial flux was considered as the theoretical initial value of flux calculated thanks to the Darcy Law using the initial water permeability of the membrane and the TMP applied during the filtration. A pseudo stable permeate flux was supposed to be reached when the decrease in flux was less than 1% of the initial flux over a filtration time of 1 h. It could take 8–9 h to obtain this pseudo stable flux in the present study.

3.3. Analytical methods

3.3.1. Water matrix characterization

The composition of MBR effluents was measured by the following methods as reported in a previous publication (Lan et al., 2017). Salts concentrations were measured by ionic chromatog raphy using an ICS 3000 system (Dionex, France). The concentra tions of anions and cations were analysed with two columns (Thermo Scientific, Dionex): IonPacTM AS11 (mobile phase: 95% of 5 mM NaOH and 5% of 100 mM NaOH) and IonPacTM CS12 (mobile phase: $CH_4O_3SO_3$ 20 mM), respectively. In this mobile phase, all H_3PO_4, $H_2PO_4^-$, HPO_4^{2-} and PO_4^{3-} present in the solution were referred to as PO_4^{3-}.

Concentration of Ciprofloxacin (CIP) as target pharmaceutical was monitored by HPLC MS/MS (Waters Acquity™ Ultra performance LC QuattroPremier XE Micromass MS Technologies) by LPTC in Bordeaux (Université de Bordeaux 1, EPOC, LPTC, UMR 5805, Laboratoire de Physico et Toxico Chimie de l'Environnement) after addition of specific internal standards and purification by solid phase extraction (SPE, Oasis HLBTM, 200 mg, 6 cc, Waters®). The quantification limit for CIP is 22.3 ng L^{-1}. Residual standard devia tion is about 10%.

Total Organic Carbon (TOC) and Inorganic Carbon (IC) were measured with a TOC VCSN instrument (Shimadzu). Chemical Oxygen Demand (COD) was determined by photometry using disposable test tubes (HI93754H 25 LR from HANNA Instruments) and a HACH DR/2400 photometer.

pH (A 32908 06, Labcor Technical Sales Inc.) and conductivity (23226–523, VWR, Mississauga, Ontario) were measured. Absor bance was analysed using a spectrophotometer (Hewlett Packard 8452A) at a wavelength of 254 nm (UV_{254}) with a quartz crystal cuvette.

3.3.2. Membrane surface characterization

Virgin and fouled membranes after filtration were characterized after drying at 60 °C with a vacuum degree fixed at 0.8 bar (C3000 XF020 France, Etuves).

ATR FTIR spectra (Attenuated Total Reflection Fourier Trans form InfraRed spectroscopy) were obtained with a Thermo Nicolet Nexus 670 apparatus (USA). The sample was placed on a diamond crystal substrate and the analytical depth was approximately two μm.

Membrane surface morphology was examined with a Scanning Electron Microscope (SEM, Hitachi Table top Microscope TM 1000) interfaced with an Energy Dispersive X ray (EDX) spectroscopy system (Thermo Fisher). Membrane samples were coated with a thin layer of gold before SEM analysis. EDX measurements were performed at different locations of the membrane surface, in order to obtain a comprehensive elemental composition. Elemental analysis began with sodium.

4. Results and discussion

4.1. Variation of fluxes and pseudo stable fluxes

Filtrations were performed under a constant transmembrane pressure from 3 to 35 bar. Fig. 1 shows the flux over time from the beginning of the experiment (including concentration step) in selected filtrations under different transmembrane pressures (TMP). During filtrations at low TMP (3 and 5 bar), fluxes remained stable over the entire filtration period and the pseudo stable fluxes

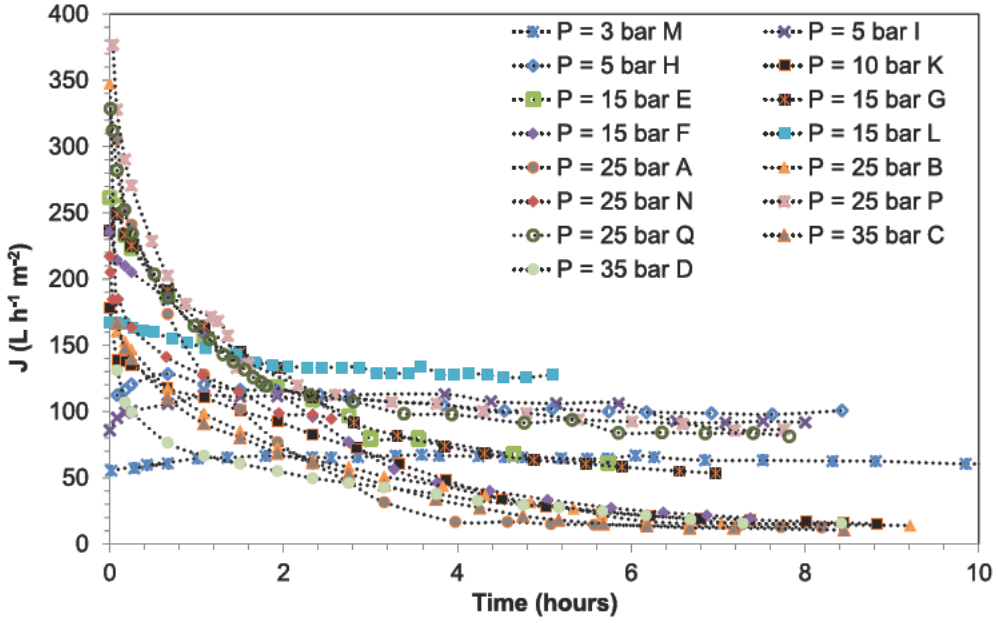

Fig. 1. Evolution of permeate flux of all filtrations over filtration time at various transmembrane pressures.

increased with the TMP. These results indicated that if a fouling occurred in this range of applied pressures, it was very low and did not lead to detectable flux decline. On the other hand, when fil trations were operated at transmembrane pressures of 10–35 bar, fluxes declined at early periods of filtration, which revealed the occurrence of noticeable fouling. Three typical stable fluxes were observed. In the first case (25 bar, Q) the flux stabilized within 82 L h^{-1} m^{-2}. Hence, the stable fluxes at 5 bar and 25 bar reached almost the same value while we were expecting a noticeable rise in stable flux at 25 bar. This result is due to the appearance of a fouling layer at 25 bar while negligible fouling was observed at 5 bar. This flux limitation indicates an expected limiting flux, around 80 L h^{-1} m^{-2}. Nevertheless, in a second group of filtrations, 10 bar K, 25 bar A and 35 bar C, the stable fluxes with values around 10 L h^{-1} m^{-2} are significantly lower, even below the flux obtained at 5 bar. The limiting flux is expected to be 10 L h^{-1} m^{-2}. The third situation is observed in filtration G that reached an intermediate stable flux of 53 L h^{-1} m^{-2}.

The difference in expected limiting fluxes and stable fluxes can be attributed to the changes in MBR effluent characteristics, such as pH, ionic strength, and divalent cation concentrations according to the study of Tang et al. (Tang et al., 2009a; Tang and Leckie, 2007). Considering this variability in MBR effluents sampled, it was not possible to perform meaningful replicate. After all, filtrations H and I (5 bar), E and G (15 bar), A and B (25 bar), P and Q (25 bar) and C and D (35 bar) could be considered as duplicate due to the fact that NF feeds were similar in concentrations and TMP applied was the same. In these cases, results exhibit similar stable flux.

In order to identify the key factors that induce severe fouling and low stable fluxes in the MBR effluent matrix, we firstly tried to use the working diagram developed in our previous study (Lan et al., 2017). Fig. 2 plots the experimental stable fluxes on the NF working diagram for independent MBR effluent filtrations. The description of all regions in this diagram was proposed in the introduction. One can observe that filtrations M, H at 3 and 5 bar are in the non fouling region, which correlate well with the experi mental observation that no detectable flux reduction appeared in Fig. 1. The filtration L (15 bar) that reaches a lower stable flux than the initial flux at 15 bar (deduced from initial membrane water permeability and TMP applied of 15 bar according Darcy Law) may correspond to organics fouling (Filtration L located in region of organics fouling in Fig. 2). By contrast, filtrations K, F, A, B, C, D for

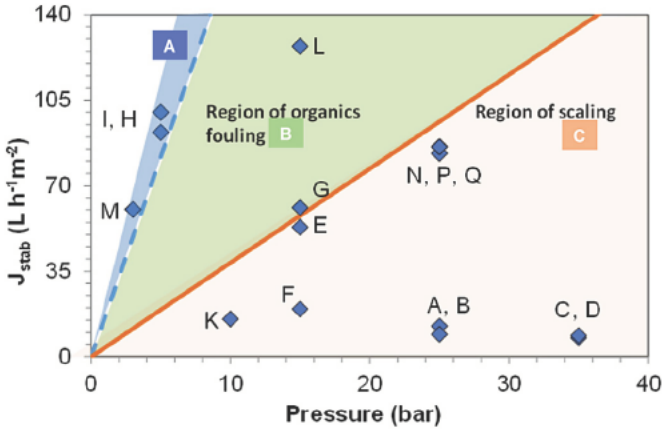

Fig. 2. Stable fluxes in independent filtrations of MBR effluents at various trans-membrane pressures. A, B … Q are the serial name of filtrations (Table 1). The dashed blue line corresponds to the average initial pure water permeability of membranes. The full red line is the permeability before scaling (Lan et al., 2017). (For interpretation of the references to colour in this figure legend, the reader is referred to the Web version of this article.)

which rather low stable fluxes (around 10 L h^{-1} m^{-2}) were observed, are located in the scaling region. The combined effect of organics fouling and calcium phosphate scaling is expected in this case, according to the diagram analysis and literature (Dahdal et al., 2016; Rathinam et al., 2018). Finally, filtrations Q, P (flux around 80 L h^{-1} m^{-2}) and E and G (flux around 50 L h^{-1} m^{-2}) are located at the boundary between organics fouling and scaling regions. They will require further study to understand the fouling mechanisms and the relation to the stable flux.

Simultaneously to flux monitoring, removal performances of the NF membrane were estimated (see Tables 3 and 4 in supplementary information section). Removal of Ciprofloxacin (CIP) as target pharmaceutical has been quantified. CIP is an antibiotic widely used in hospital and exhibiting bio resistance in MBR process. Consequently, CIP is one of the major pharmaceutical in the MBR effluent sampled for the present study (concentration in MBR ef fluents up to 0.07 mg L^{-1}). In Fig. 2 region A, CIP rejection was ranging from 33 to 57% when in region C it reached 71–100% (see Table 5 in supplementary information section). At the same time, in region C (including filtration serials F, K, A, B, C and D) the range of COD removal was 88–99% and the one of TOC 96–99%.

4.2. Fouling layer characterization and link between foulants composition and stable flux

The physico chemical properties of the fouling layer were ana lysed by FTIR and SEM EDX in order to verify the inference of fouling mechanisms from the working diagram analysis. Moreover, we looked for the link between foulants compositions and stable fluxes, which should allow us to confirm the relationship between water matrix characteristics and stable fluxes.

4.2.1. Fouling layer characterization by ATR FTIR analysis

Fig. 3 presents the ATR FTIR spectra of pristine and fouled membranes. The spectra of pristine NE70 membrane is character istic of an active polyamide top layer: peaks at 1630 cm^{-1}, with a polysulfone sub layer: peaks at 1587, 1504, and 1488 cm^{-1}, in addition to a coating layer (top of the active polyamide layer) with a characteristic absorbance over 3000 2900 cm^{-1} (Tang et al.,

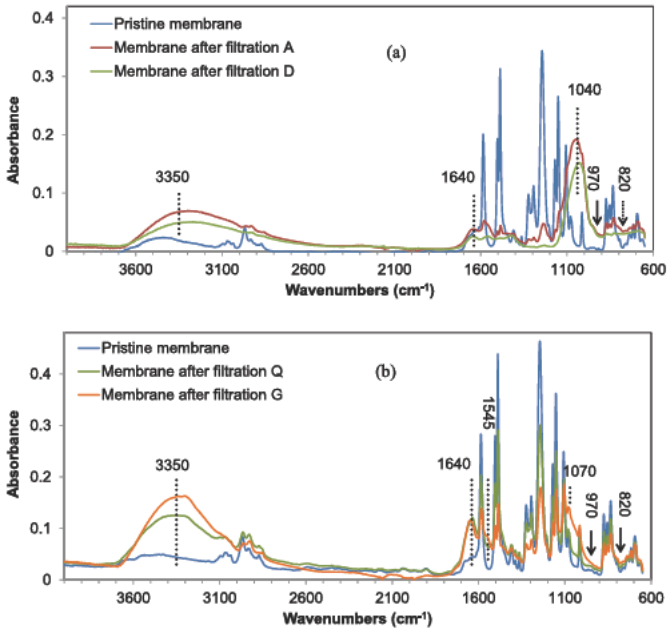

Fig. 3. FTIR spectra of pristine and fouled membranes after filtrations.

2009b).

The spectra of fouled membranes after filtrations A and D (low stable flux: 10 L h^{-1}m^{-2}) shows great resemblance to the one of membrane fouled by colloidal silica, organics and calcium phos phate scaling (Lan et al., 2017). Peaks at 3300 cm^{-1} and 1545 cm^{-1} corresponding to N–H stretching and bending vibrations, together with a peak at 1647 cm^{-1} associated with the stretching vibration of C O, indicate the presence of colloidal organics (Jarusutthirak et al., 2002; Nguyen et al., 2009). In addition, OH stretching and the Si–OH group vibration are observed at 970 cm^{-1} and 3700 3200 cm^{-1} (Lee et al., 2004); the absorbance around 820 cm^{-1} is associated with the symmetric bond stretching vibration of the Si–O–Si network (Muroya, 1999). These absorbance peaks imply the presence of colloidal silica fouling (Gorzalski and Coronell, 2014). The wide and intensive peak at 1049 cm^{-1} is reported to be characteristic of phosphate (including PO_4^{3-}, HPO_4^{2-}, HPO_4^{-1}) and crystallized calcium phosphate (Elzinga and Sparks, 2007; Ślósarczyk et al., 1997; Theophile, 2012), which suggests the pres ence of calcium phosphate scaling on the fouled membrane surface. By comparison, the absorbance band around 1445 cm^{-1}, which corresponds to calcium carbonate, is very weak, indicating that carbonate was not the main foulant.

For the fouled membranes after the filtrations Q (stable flux: 82 L h^{-1}m^{-2}), we only observed the absorbance of organics and silica foulants: peaks at 3300, 1545 and 1647 cm^{-1} corresponding to organic fouling, 970 and 820 cm^{-1} attributing to silica fouling. The absence of peak in the region 1030 1100 cm^{-1} indicates that no calcium and phosphate scaling appear on the membrane surface. On the other hand, membrane after filtration G (stable flux: 53 L h^{-1}m^{-2}) presents an 'intermediate' fouling layer including organic and silica fouling and probably scaling (peak at 1070 cm^{-1}) whilst the absorbance of scaling is less intensive compared to that of the membranes after filtrations A and D.

4.2.2. Fouling layer characterization by SEM EDX analysis

To further verify the fouling mechanisms and understand the link between them and stable fluxes, SEM analyses were performed on membrane surfaces and cross section to characterize the fouling layer's structure and morphology (Fig. 4 in supplementary infor mation section). Combined with SEM, EDX was applied to analyse the elemental compositions on membrane surfaces. The weight percentages of main elements are reported in Table 3. These data were used in the present study to evaluate the relative distribution of Calcium, Phosphate and Silica on each fouled membrane surface, referring to Sulphur, which is taken as a standard (membrane material shows 100% of sulphur).

We compared the micrographs of the pristine membrane and membranes after filtration A and D, which were likely to be fouled by colloidal silica, organics and calcium phosphate scaling accord ing FTIR analysis. A variety of "bright" particles appears, evenly distributed over the entire fouled membrane surfaces. In particular, for the membrane after filtration D, "bright" particles are sharp and the size of them varies from 0.5 μm to 1 μm. The cross section image shows that the foulant layer thickness is relatively uni form, around 2 μm.

From the EDX analysis (Table 3), sulphur is the only element detected on the pristine membrane surface, while on the fouled membranes after filtrations A and D; Ca and P are the major ele ments detected. It can be observed that after filtration D, most of the measurements were unable to detect sulphur characterizing membrane material, which is probably due to a fouling layer, thicker than the depth of EDX analysis. Furthermore, we have to notice that Carbon, characterizing organics, was not quantified by the EDX instrument because of its limitation, but from FTIR results organics and colloidal silica fouling was detected on these mem brane samples. However, combination of the different tests con ducted let us assume that after filtrations A and D the main fouling mechanism is calcium and phosphate scaling, with a low contri bution to the decrease in flux of organics and colloidal silica fouling (absence or low silicon percentage on the membrane surface after filtrations A and D see Table 3). Moreover, it is worth noticing that although the percentage of Ca on the membrane surface after filtration D is higher than the Ca percentage after filtration A, the stable fluxes reached during these two filtrations were similar.

When we focus on the micrograph and element percentage of the membrane surface after filtration Q (obtaining a higher stable flux), it is found that a homogenous dark layer covered the fouled membrane surface and only silicon and sulphur were detected by EDX, in absence of calcium and phosphorus. These observations confirm the results from the FTIR analysis that the membrane was only fouled by organics and silica.

In the case of filtration G, an uneven surface was observed and the presence of silicon, calcium and phosphate was detected, indicating that scaling occurred during this filtration whilst the stable flux was greater than that of filtrations A and D. For further understanding, other fouled membranes at this TMP, whilst lower in stable flux (15 L h^{-1}m^{-2}, filtration F) were characterized. Again, an uneven fouling layer was observed. However, the element percentages of calcium and phosphate are higher than that of filtration G.

To go further in the analysis of the membrane surface coverage by scalants, Fig. 4 plots the percentage of calcium and phosphorus (scalants) versus the corresponding sulphur percentage (mem brane) on each location analysed on a membrane surface. Pristine and fouled membranes after filtrations A, D, G and F were consid ered. As mentioned previously, the points corresponding to the pristine membrane are located at 100% sulphur and 0% calcium or phosphate in both Fig. 4 (a) and (b). It was found that after filtra tions A and D, the percentages of calcium and phosphorus on the membrane surface are relatively uniform (for example Ca 75% and P 25% on different locations after filtration D), indicating their even distribution on the membrane surface. On the other hand, fouled membranes after filtrations G and F exhibited various percentages of calcium and phosphorus as a function of the measurement location, which means that the distribution of scalants is uneven. The percentages of calcium and phosphorus vary from 0 to 50% on

Table 3
EDX analysis at different locations on the membrane surface before and after each filtration.

Membrane	Pristine	Q	G	F	A	D	I
J_{stab} (L h ^{1}m ^{2})		82	53	15	10	10	84
Element	Average weight % from the different locations on membrane surface (each line results from an average of 4 or 5 spots)						
Sulphur	100	90.8 ± 3.3	52.7 ± 32.7	43.0 ± 7.0	8.9 ± 2.52	3.2 ± 9.6	87.6 ± 18.8
Silicon	0	9.2 ± 3.3	8.7 ± 7.0	4.8 ± 12.8	2.8 ± 0.80	0	12.1 ± 7.2
Calcium	0	0	22.8 ± 20.5	38.9 ± 4.6	55.8 ± 7.8	73.6 ± 10.5	6.3 ± 12.6
phosphorus	0	0	12 ± 15.7	10.2 ± 8.8	24.5 ± 3.46	23.2 ± 3.5	0

*large deviations come from high variability of the element on the membrane surface depending on the spot analysed.

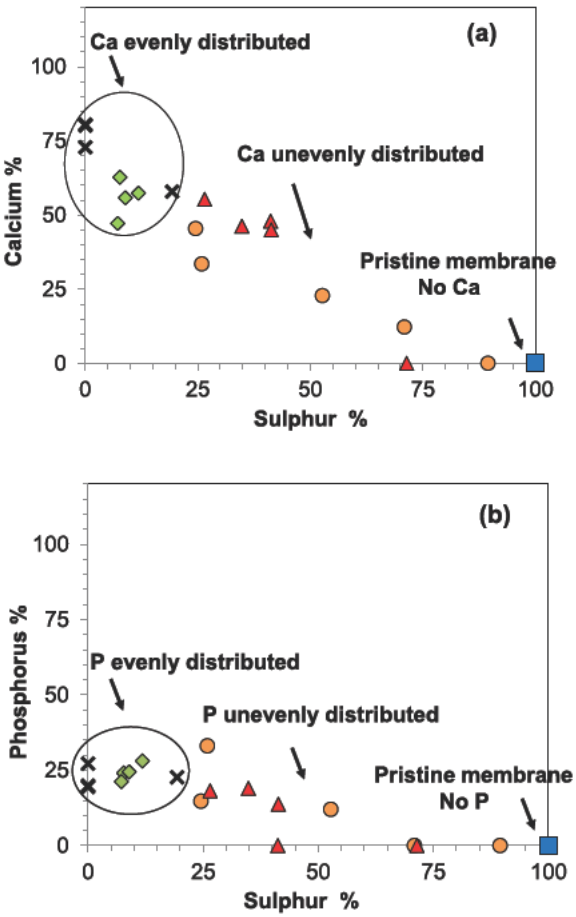

Fig. 4. Surface elemental percentages of calcium versus sulphur (a) and phosphorus versus sulphur (b) on each analysis location on pristine and fouled membranes after filtration A ◆, D ×, G ● and F ▲.

the membrane surface after filtration G.

4.2.3. Relation between fouling layer compositions and NF stable fluxes

Fig. 5 illustrates the relationship between the average Ca/S and P/S element ratio on the membrane surface and stable fluxes. It can be observed that stable fluxes decrease with the increase in the Ca/S and P/S ratio in filtrations Q, I, G and F, corresponding to cases from absence to the uneven distribution of scalants on the membrane surface. For filtrations A and D where the scalants were evenly distributed, although an increase in the Ca/S and P/S ratio, stable fluxes were almost equal. Considering membrane permeability (to take into account different TMP used in filtrations A and D), this one was equal to 0.5 L $h^{-1}m^{-2}bar^{-1}$ at the end of filtration A and to 0.24 L $h^{-1}m^{-2}bar^{-1}$ at the end of filtration D, values very similar. If we assume that the greater percentages of calcium and phosphorus on the membrane probably contribute to a thicker scaling layer, we can then conclude that the thickness of the scalant layer seems to have less impact on membrane permeability reduction than its distribution, from patchy to even.

According to the discussion above, the various fouling mechanisms lead to diverse stable fluxes. The combined effect of organic, silica fouling and homogenous calcium phosphate scaling leads to extremely low stable fluxes (1%–2% of theoretical initial flux). In these conditions (e.g. filtrations A and D), scalants are evenly distributed on the membrane surface and the stable flux magnitude is unlikely to be affected by a further development of a scaling layer on the membrane surface (increase in percentages of Ca and P). When this type of fouling occurs, the expected limiting flux for NF of MBR effluents is around 10 L $h^{-1}m^{-2}$. Organic and silica fouling in the absence of calcium and phosphate scaling induce greater stable fluxes (e.g. the filtration Q). The expected limiting flux is approximately 86 L $h^{-1}m^{-2}$ for this type of fouling. When calcium and phosphate scaling, distributed unevenly on the membrane surface, the values of stable fluxes are between the values of the two conditions above (10–86 L $h^{-1}m^{-2}$). The stable fluxes then depend on the percentage of calcium and phosphorus on the membrane surface, e.g. filtrations G and F.

4.3. Relation between scalant ions concentrations in MBR effluent and NF stable fluxes

Previous results showing that calcium and phosphate are the main foulants responsible for flux decline, we investigate in this section the key parameters in MBR effluents inducing scaling. The precipitation of calcium and phosphate components depends on the supersaturation ratio on the membrane surface (S_m, equation (5)) and consequently on the concentration of calcium and phosphate in the solution. Fig. 6 plots stable fluxes referred back to the unit of transmembrane pressure (to take into account the impact of the flow on the quantity of matter brought to the membrane surface) versus calcium and phosphate concentrations in corresponding MBR effluent.

Except for filtrations M, H and I where no noticeable fouling occurred, we found that in most of the filtrations (e.g. G, F and A), stable fluxes per unit of pressure decreased with the increase in calcium and phosphate concentrations. However, the stable fluxes

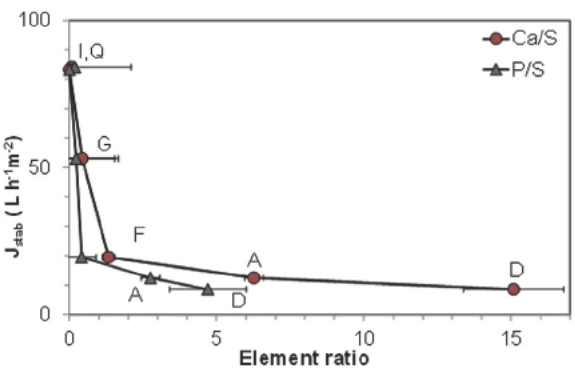

Fig. 5. Relationship between element ratio (Ca/S, P/S) on the membrane surface and pseudo stable fluxes. A, D, F, H, G, and I are the serial names of filtrations (see Table 1).

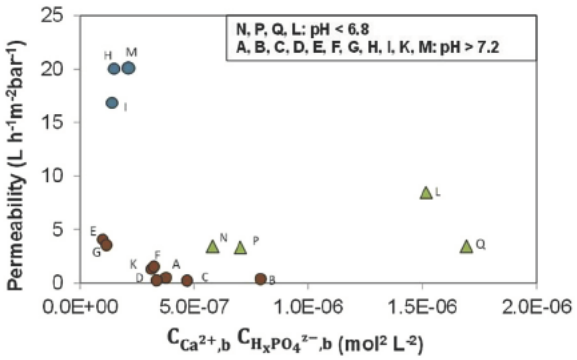

Fig. 6. Membrane permeability (pseudo stable fluxes referred back to the unit of pressure) versus calcium and phosphate concentration product in MBR effluent. A, B … Q are the serial name of filtrations (see Table 1).

in filtrations P and Q maintained relatively high values, even though calcium and phosphate concentrations in the feed matrix were higher than concentration in other effluents. It seems that not only the concentration of scalant ions, but also other critical factors, affect the level of stable fluxes. As we indicated in section 2, the main species of phosphate is dihydrogen phosphate ($H_2PO_4^-$) when the pH is below 7.2 and hydrogen phosphate (HPO_4^-) for pH above 7.2. pH values of feed matrix in filtrations P and Q were 6.74 and 6.80 respectively where phosphate is in $H_2PO_4^-$ form, whilst for the other filtrations, the feed matrix pH ranged from 7.45 to 7.95 (and 7.20 to 8.27 after FRV 5) where the phosphate form is HPO_4^-. Moreover, from Table 1 in supplementary information, one can notice that all calcium and hydrogen phosphate (HPO_4^-) compounds have slightly lower solubility than calcium and dihydrogen phosphate ($H_2PO_4^-$) compounds. For example, the solubility of $CaHPO_4$ is 10^5 times lower than that of $Ca(H_2PO_4)_2$.

Thus, we found that:

(1) When the major phosphate form is HPO_4^- in the MBR effluents (pH > 7.2), scaling occurred even though calcium and phosphate concentrations are relatively low (e.g. filtrations G, F and A). This is due to the extremely low solubility of calcium hydrogen phosphate compounds. In these conditions, an increase in concentration of calcium and phosphate leads to their abundant precipitation on the membrane surface. The membrane surface area occupied by these scalants then increases, leading to lower stable fluxes. When the entire membrane surface is occupied by scalants, extremely low limiting fluxes are observed. In this case, higher scalant ion concentrations in MBR effluent would no longer affect the stable flux (e.g. filtration B).

(2) When the major phosphate form is $H_2PO_4^-$ in the MBR effluents (pH < 7.2), scaling only appears if the calcium and phosphate concentration product exceeds the thermodynamic solubility product (K_{sp}) of the corresponding calcium and dihydrogen phosphate compounds. Since their K_{sp} is much higher, scaling is negligible at the given calcium and phosphate concentrations (filtrations P and Q). The absence of less permeable layer of scalants on the membrane surface results in a greater limiting flux.

(3) Stable fluxes of NF for purification of MBR effluents are sensitive to pH: a slight pH variation from 6.8 to 7.2 results in severe fouling and low stable fluxes.

4.4. Link between organics and scalant ions concentrations in MBR effluents and stable fluxes

Since organic fouling or combination of it with calcium and phosphate scaling are two main fouling mechanisms during NF of MBR effluents, we propose in the following to establish the link between their concentrations in MBR effluents and stable fluxes.

4.4.1. Qualitative link between organics concentration in MBR effluents and stable fluxes (pH < 6.8)

In the case of effluents the pH of which is lower than 6.8 (filtrations N, P, Q and L), it has been demonstrated that scaling is negligible in the TMP range tested (0–25 bar). We then propose to correlate organics concentration in MBR effluent and stable fluxes. Herein, organics concentration was evaluated in the NF retentate (MBR effluent at VRF 5 in the concentration loop of the NF system) by UV absorbance at the wavelength of 254 nm (UV_{254}), COD and TOC.

The results reported on Fig. 7 show a decrease in membrane permeability ($J_{stab}/\Delta P$) when UV_{254}, TOC and COD increase until a plateau value was reached. This confirms the role of the organics concentration in the value of the stable fluxes for filtrations at pH < 6.8. If we go further in data analysis, we can say, on one hand, that among total organic compounds present in MBR effluent, aromatic ones are more concentrated in the feed of filtration N by comparison to the feed of filtration P. On the other hand, filtration P feed is the most concentrated in terms of general compounds that could be chemically oxidized. We could expect an effect of these differences in feed composition on the pseudo stable flux reached, which was not observed in the tested conditions as soon as organics in the influent reached a certain concentration. Hence, in the present study the distinction of the different fractions of organic matter did not provide additional information on the influence of organics composition of the MBR effluent on NF flux.

4.4.2. Quantitative link between scalant ions concentrations in MBR effluents and stable fluxes (pH > 7.2)

The following model puts forward the variation of stable fluxes with calcium and phosphate concentrations in MBR effluents.

As discussed in section 2, the supersaturation ratio on the membrane surface can be expressed as equation (7).

$$S_m \quad \frac{C_{Ca^{2+},b}\, C_{H_xPO_4^{z-},b}\, CP_{Ca^{2+}}\, CP_{H_xPO_4^{z-}}}{K_{sp}} \tag{7}$$

where, $C_{Ca^{2+},b}$ and $C_{H_xPO_4^{z-},b}$ are the concentrations of calcium and phosphate in the bulk, CP is the concentration polarization degree; K_{sp} is the thermodynamic solubility product of the scalant compound.

The concentration polarization degree for each ion is written as equations (10) and (11) (Zydney, 1997; Wei et al., 2010) deduced from the Film theory (Eq. (2)) and the definition of the observed rejection R_{Obs} and the membrane rejection R_m as follow:

$$R_{Obs} \quad 1 \quad \frac{C_p}{C_b} \tag{8}$$

$$R_m \quad 1 \quad \frac{C_p}{C_m} \tag{9}$$

$$CP_{H_xPO_4^{z-}} \quad \frac{C_{H_xPO_4^{z-},m}}{C_{H_xPO_4^{z-},b}} \left(1 \quad R_{Obs(H_xPO_4^{z-})}\right) + R_{Obs(H_xPO_4^{z-})} exp \quad \frac{J_{stab}}{k_{H_xPO_4^{z-}}} \tag{10}$$

$$CP_{Ca^{2+}} \quad \frac{C_{Ca^{2+},m}}{C_{Ca^{2+},b}} \quad (1 \quad R_{Obs(Ca^{2+})}) + R_{Obs(Ca^{2+})} exp\left(\frac{J_{stab}}{k_{Ca^{2+}}}\right) \tag{11}$$

Where $C_{Ca^{2+},m}$, $C_{Ca^{2+},b}$ and $C_{H_xPO_4^{z-},m}$,$C_{H_xPO_4^{z-},b}$ are calcium and phosphate concentrations on the membrane surface and in the bulk, respectively; J_{stab} is the stable permeate flux; $R_{Obs(Ca^{2+})}$ and $R_{Obs(H_xPO_4^{z-})}$ are the observed ion rejections; $k_{H_xPO_4^{z-}}$ and $k_{Ca^{2+}}$ are the mass transfer coefficients in the boundary layer of phosphate and calcium, respectively.

Since Ca^{2+} and PO_4^{3-} are multivalent salts, the rejections of them by NF membranes tend to 1 in most conditions (experimental rejection >90% in this work). In this case, equations (10) and (11) can be simplified to equations (12) and (13) as follows:

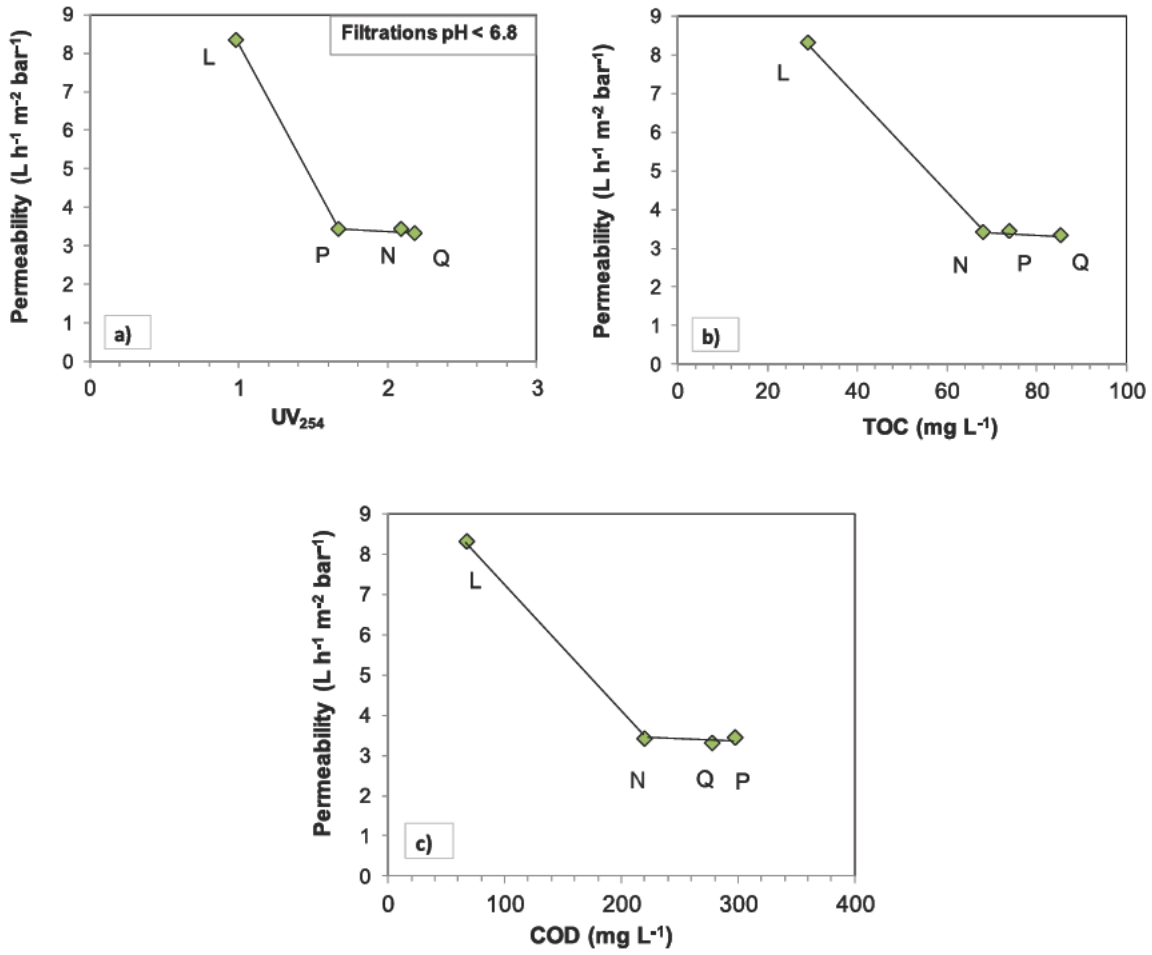

Fig. 7. Membrane permeability (pseudo stable fluxes referred back to the unit of pressure) versus a) UV absorbance at 254 nm, b) TOC and c) COD in MBR effluent at VRF 5 (filtrations at pH < 6.8).

$$CP_{H_xPO_4^z} \quad exp\left(\frac{J_{stab}}{k_{H_xPO_4^z}}\right) \tag{12}$$

$$CP_{Ca^{2+}} \quad exp\left(\frac{J_{stab}}{k_{Ca^{2+}}}\right) \tag{13}$$

Combining equations (7), (12) and (13), the supersaturation ratio on the membrane surface can be expressed as:

$$S_m \quad \frac{C_{Ca^{2+},b}\, C_{H_xPO_4^z,b}\; exp\left(\frac{J_{stab}}{k_{Ca^{2+}}}\right) exp\left(\frac{J_{stab}}{k_{H_xPO_4^z}}\right)}{K_{sp}} \tag{14}$$

Chemical precipitation potentials might be obtained for a wide range of salts using software packages such as Avista, Phreeqc, Minteq, which are based on equilibrium thermodynamics.

From equation (14), the numerical link between stable fluxes and calcium and phosphate concentrations in MBR effluents is obtained:

$$J_{stab} \quad \ln(S_m K_{sp}) \frac{k_{H_xPO_4^z}\, k_{Ca^{2+}}}{k_{H_xPO_4^z} + k_{Ca^{2+}}} \frac{k_{H_xPO_4^z}\, k_{Ca^{2+}}}{k_{H_xPO_4^z} + k_{Ca^{2+}}} \ln\left(C_{Ca^{2+},b}\, C_{H_xPO_4^z,b}\right) \tag{15}$$

This relation can be written as equation (16)

$$J_{stab} \quad AB_k \quad B_k \ln\left(C_{Ca^{2+},b}\, C_{H_xPO_4^z,b}\right) \tag{16}$$

$$A \quad \ln(S_m K_{sp}) \tag{17}$$

$$B_k \quad \frac{k_{H_xPO_4^z}\, k_{Ca^{2+}}}{k_{H_xPO_4^z} + k_{Ca^{2+}}} \tag{18}$$

where coefficient A relates to the supersaturation ratio on the membrane surface and the thermodynamic solubility product of the scalant compounds; B_k is a constant associated with mass transfer coefficients of calcium and phosphate.

Based on the fouling mechanisms study, this relationship is valid when scaling appears until it becomes homogenous. Fig. 8 illustrates the relationship between J_{stab} and $\ln\left(C_{Ca^{2+},b}\, C_{H_xPO_4^z,b}\right)$ according to equation (16) for the filtrations subject to scaling (pH > 7.2). A linear relationship is visible, except for filtrations H, I, M and B. Since no considerable fouling occurred in filtrations H, I and M, their stable fluxes are independent to the scalant ions concentrations. For filtration B, this particular case confirms that the relationship (16) is not valid to describe stable fluxes when scaling has reached a homogenous layer on the membrane surface, the stable flux therefore, not correlated to the concentration of ions.

Therefore, due to the results reported on Fig. 8, the NF stable fluxes can be estimated in various MBR effluents collected over a

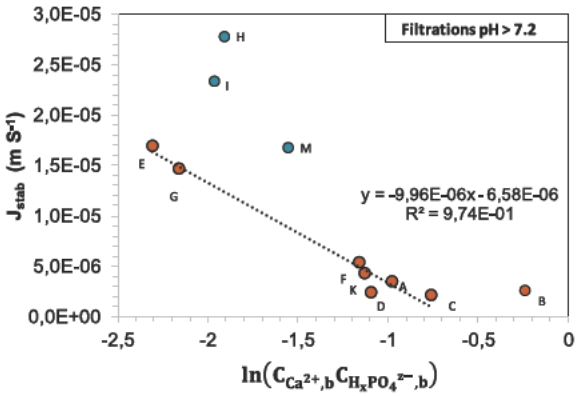

Fig. 8. Relationship between stable fluxes and the calcium and phosphate concentrations in effluent matrix pH > 7.2.

period of 145 days on a system treating hospital wastewater (for the variation of composition refer to Table 1), when the predominant fouling responsible for the flux decline, calcium phosphate scaling, appears (pH > 7.2).

5. Conclusion

This study aimed to investigate the effect of real MBR effluent chemistry on performances of NF used as tertiary treatment. The impact of the water matrix on the NF stabilized flux and on fouling types and degrees was studied, and a quantitative link between the concentration of matrix components and stable fluxes was studied.

Two types of fouling were observed during NF of MBR effluents collected over a period of 145 days. The appearance of these two fouling mechanisms strongly depends on MBR pH (from 6.05 to 8.27 after FRV 5 in all MBR effluents considered in this study): in the range 6.05 < pH < 6.80, silica and colloidal organic fouling was observed when a combination of silica and colloidal organic fouling and calcium phosphate scaling occurred in the range 7.20 < pH < 8.27. When the membrane underwent organic fouling and scaling, low stable fluxes from 60 to 10 $L\,h^{-1}m^{-2}$ were observed. This value depends on calcium and phosphate percent ages and distribution on the fouled membrane surface. Extremely low limiting fluxes (around 10 $L\,h^{-1}m^{-2}$, 1%–2% of theoretical initial flux calculated from the membrane water permeability and the TMP applied) appeared when calcium and phosphate scaling evenly occupied the entire membrane surface. By comparison, relatively greater stable fluxes (120 80 $L\,h^{-1}m^{-2}$) were obtained when only silica and organic fouling occurred.

The form of phosphate is responsible for the presence of scaling. For pH values higher than 7.2, phosphate is present as hydrogen phosphate. The corresponding salt: calcium hydrogen phosphate, exhibits an extremely low solubility. Scaling occurs even at low calcium and phosphate concentrations in the water matrix. Consequently, in this pH range, NF stable fluxes were subject to calcium and phosphate concentrations in solution.

The quantitative link between stable fluxes and calcium and phosphate concentrations was established, that correlates well with experimental results. Therefore, NF stable flux values for filtration of various MBR effluents can be calculated from calcium and phosphate concentrations after judgement of effluents' pH.

Acknowledgements

The authors would like to thank the China Scholarship Council for its financial support. They are also grateful to the coordinator of the PANACEE Project supported by ANR, French National Research Agency, for allowing them access to MBR effluents.

Appendix A. Supplementary data

Supplementary data related to this article can be found at https://doi.org/10.1016/j.watres.2018.09.004.

References

Aimar, P., Field, R., 1992. Limiting flux in membrane separations: a model based on the viscosity dependency of the mass transfer coefficient. Chem. Eng. Sci. 47, 579 586. https://doi.org/10.1016/0009-2509(92)80008-Z.

Alturki, A.A., Tadkaew, N., McDonald, J.A., Khan, S.J., Price, W.E., Nghiem, L.D., 2010. Combining MBR and NF/RO membrane filtration for the removal of trace organics in indirect potable water reuse applications. J. Membr. Sci. 365, 206 215. https://doi.org/10.1016/j.memsci.2010.09.008.

Antony, A., Low, J.H., Gray, S., Childress, A.E., Le-Clech, P., Leslie, G., 2011. Scale formation and control in high pressure membrane water treatment systems: a review. J. Membr. Sci. 383, 1 16. https://doi.org/10.1016/j.memsci.2011.08.054.

Bacchin, P., Aimar, P., Field, R.W., 2006. Critical and sustainable fluxes: theory, experiments and applications. J. Membr. Sci. 281, 42 69. https://doi.org/10.1016/j.memsci.2006.04.014.

Beier, S., Cramer, C., Koster, S., Mauer, C., Palmowski, L., Schroder, H.F., Pinnekamp, J., 2011. Full scale membrane bioreactor treatment of hospital wastewater as forerunner for hot-spot wastewater treatment solutions in high density urban areas. Water Sci. Technol. 63, 66 71. https://doi.org/10.2166/wst.2011.010.

Contreras, A.E., Kim, A., Li, Q., 2009. Combined fouling of nanofiltration membranes: mechanisms and effect of organic matter. J. Membr. Sci. 327, 87 95. https://doi.org/10.1016/j.memsci.2008.11.030.

Dahdal, Y.N., Oren, Y., Schwahn, D., Pipich, V., Herzberg, M., Ying, W., Kasher, R., Rapaport, H., 2016. Biopolymer-induced calcium phosphate scaling in membrane-based water treatment systems: Langmuir model films studies. Colloids Surfaces B Biointerfaces 141, 233 242.

DiGiano, F.A., Arweiler, S., Riddick, J.A., 2000. Alternative tests for evaluating NF fouling. J. Am. Water Works Assoc. 103 115.

Elzinga, E.J., Sparks, D.L., 2007. Phosphate adsorption onto hematite: an in situ ATR-FTIR investigation of the effects of pH and loading level on the mode of phosphate surface complexation. J. Colloid Interface Sci. 308, 53 70. https://doi.org/10.1016/j.jcis.2006.12.061.

Gorzalski, A.S., Coronell, O., 2014. Fouling of nanofiltration membranes in full- and bench-scale systems treating groundwater containing silica. J. Membr. Sci. 468, 349 359. https://doi.org/10.1016/j.memsci.2014.06.013.

Greenberg, G., Hasson, D., Semiat, R., 2005. Limits of RO recovery imposed by calcium phosphate precipitation. Desalination, Desalination and the Environment 183, 273 288. https://doi.org/10.1016/j.desal.2005.04.026.

Hashlamon, A., Mohammad, A.W., Ahmad, A., 2016. The effect of wastewater pretreatment on nanofiltration membrane performance. J. Water Reuse Desalination 8, 45 52. https://doi.org/10.2166/wrd.2016.083.

Jacob, M., Guigui, C., Cabassud, C., Darras, H., Lavison, G., Moulin, L., 2010. Performances of RO and NF processes for wastewater reuse: tertiary treatment after a conventional activated sludge or a membrane bioreactor. Desalination 250, 833 839. https://doi.org/10.1016/j.desal.2008.11.052.

Jarusutthirak, C., Amy, G., Croué, J.-P., 2002. Fouling characteristics of wastewater effluent organic matter (EfOM) isolates on NF and UF membranes. Desalination 145, 247 255. https://doi.org/10.1016/S0011-9164(02)00419-8.

Judd, S.J., 2016. The status of industrial and municipal effluent treatment with membrane bioreactor technology. SI New Concepts Membr. React. Membr. Des. Tissue Eng. 305, 37 45. https://doi.org/10.1016/j.cej.2015.08.141.

Kovalova, L., Siegrist, H., Singer, H., Wittmer, A., McArdell, C.S., 2012. Hospital wastewater treatment by membrane bioreactor: performance and efficiency for organic micropollutant elimination. Environ. Sci. Technol. 46, 1536 1545. https://doi.org/10.1021/es203495d.

Lan, Y., Groenen-Serrano, K., Coetsier, C., Causserand, C., 2017. Fouling control using critical, threshold and limiting fluxes concepts for cross-flow NF of a complex matrix: membrane BioReactor effluent. J. Membr. Sci. 524, 288 298. https://doi.org/10.1016/j.memsci.2016.11.001.

Lee, N., Amy, G., Croué, J.-P., Buisson, H., 2004. Identification and understanding of fouling in low-pressure membrane (MF/UF) filtration by natural organic matter (NOM). Water Res. 38, 4511 4523. https://doi.org/10.1016/j.watres.2004.08.013.

Levchenko, S., Freger, V., 2016. Breaking the symmetry: mitigating scaling in tertiary treatment of waste effluents using a positively charged nanofiltration membrane. Environ. Sci. Technol. Lett. 3, 339 343. https://doi.org/10.1021/acs.estlett.6b00283.

Li, Q., Elimelech, M., 2006. Synergistic effects in combined fouling of a loose nanofiltration membrane by colloidal materials and natural organic matter. J. Membr. Sci. 278, 72 82. https://doi.org/10.1016/j.memsci.2005.10.045.

McArdell, C.S., Moser, R., 2010. Separate Hospital Wastewater Treatment. EU Project NEPTUNE: Deliverable 5.4. Accessible online on. http://www.eu-neptune.org.

Meng, F., Zhang, S., Oh, Y., Zhou, Z., Shin, H.-S., Chae, S.-R., 2017. Fouling in membrane bioreactors: an updated review. Water Res. 114, 151 180. https://doi.org/10.1016/j.watres.2017.02.006.

Mohammad, A.W., Teow, Y.H., Ang, W.L., Chung, Y.T., Oatley-Radcliffe, D.L., Hilal, N., 2015. Nanofiltration membranes review: recent advances and future prospects. Desalination, State-of-the-Art Reviews in Desalination 356, 226 254. https://doi.org/10.1016/j.desal.2014.10.043.

Monnot, M., Nguyen, B., Zaviska, F., Lesage, G., Héran, M., 2017. Performance of Nanofiltration and Reverse Osmosis after Membrane Bioreactor for Urban Source-separated Urine Treatment and Water Reuse, vol. 95, pp. 18 33.

Muroya, M., 1999. Correlation between the formation of silica skeleton structure and Fourier transform reflection infrared absorption spectroscopy spectra. Colloids Surf. Physicochem. Eng. Asp. 157, 147 155. https://doi.org/10.1016/S0927-7757(99)00054-0.

Nguyen, T., Fan, L., Roddick, F.A., Harris, J.L., 2009. A comparative study of microfiltration and ultrafiltration of activated sludge-lagoon effluent. In: Desalination, International Membrane Science and Technology Conference 2007International Membrane Science and Technology Conference 2007, vol. 236, pp. 208 215. https://doi.org/10.1016/j.desal.2007.10.069.

Onesios, K.M., Yu, J.T., Bouwer, E.J., 2009. Biodegradation and removal of pharmaceuticals and personal care products in treatment systems: a review. Biodegradation 20, 441 466. https://doi.org/10.1007/s10532-008-9237-8.

Pauwels, B., Fru Ngwa, F., Deconinck, S., Verstraete, W., 2006. Effluent quality of a conventional activated sludge and a membrane bioreactor system treating hospital wastewater. Environ. Technol. 27, 395 402. https://doi.org/10.1080/09593332708618651.

Quesada, I., Gonzalez, Y., Schetrite, S., Budzinski, H., Le Menach, K., Lorain, O., Manier, N., Ait Aissa, S., Pandard, P., Abdelaziz, D., Canonge, J.-M., Albasi, C., 2015. PANACÉE : évaluation du fonctionnement d'un bioréacteur à membranes immergées traitant des effluents hospitaliers d'oncologie. Rev. Sci. Eau 28, 1. https://doi.org/10.7202/1030001ar.

Rathinam, K., Oren, Y., Petry, W., Schwahn, D., Kasher, R., 2018. Calcium phosphate scaling during wastewater desalination on oligoamide surfaces mimicking reverse osmosis and nanofiltration membranes. Water Res. 128, 217 225. https://doi.org/10.1016/j.watres.2017.10.055.

Sablani, S., Goosen, M., Al-Belushi, R., Wilf, M., 2001. Concentration polarization in ultrafiltration and reverse osmosis: a critical review. Desalination 141, 269 289. https://doi.org/10.1016/S0011-9164(01)85005-0.

Schafer, A.I., Fane, A.G., Waite, T.D., 2005. Nanofiltration-principles and Application. Elsevier Advance Technology.

Schütte, T., Niewersch, C., Wintgens, T., Tüce, S., 2015. Phosphorus recovery from sewage sludge by nanofiltration in diafiltration mode. J. Membr. Sci. 480, 74 82.

Shanmuganathan, S., Vigneswaran, S., Nguyen, T.V., Loganathan, P., Kandasamy, J., 2015. Use of nanofiltration and reverse osmosis in reclaiming micro-filtered biologically treated sewage effluent for irrigation. Desalination for Agriculture 364, 119 125. https://doi.org/10.1016/j.desal.2014.12.021.

Sherwood, T.K., Brian, P.L.T., Fisher, R.E., Dresner, L., 1965. Salt concentration at phase boundaries in desalination by reverse osmosis. Ind. Eng. Chem. Fundam. 4, 113 118. https://doi.org/10.1021/i160014a001.

Ślósarczyk, A., Paluszkiewicz, C., Gawlicki, M., Paszkiewicz, Z., 1997. The FTIR spectroscopy and QXRD studies of calcium phosphate based materials produced from the powder precursors with different CaP ratios. Ceram. Int. 23, 297 304. https://doi.org/10.1016/S0272-8842(96)00016-8.

Staff, A., 2011. Microfiltration and Ultrafiltration Membranes for Drinking Water (M53). American Water Works Association.

Tang, C.Y., Kwon, Y.-N., Leckie, J.O., 2009a. The role of foulant foulant electrostatic interaction on limiting flux for RO and NF membranes during humic acid fouling theoretical basis, experimental evidence, and AFM interaction force measurement. J. Membr. Sci. 326, 526 532. https://doi.org/10.1016/j.memsci.2008.10.043.

Tang, C.Y., Kwon, Y.-N., Leckie, J.O., 2009b. Effect of membrane chemistry and coating layer on physiochemical properties of thin film composite polyamide RO and NF membranes: I. FTIR and XPS characterization of polyamide and coating layer chemistry. Desalination 242, 149 167. https://doi.org/10.1016/j.desal.2008.04.003.

Tang, C.Y., Leckie, J.O., 2007. Membrane independent limiting flux for RO and NF membranes fouled by humic acid. Environ. Sci. Technol. 41, 4767 4773. https://doi.org/10.1021/es063105w.

Tang, F., Hu, H.-Y., Sun, L.-J., Sun, Y.-X., Shi, N., Crittenden, J.C., 2016. Fouling characteristics of reverse osmosis membranes at different positions of a full-scale plant for municipal wastewater reclamation. Water Res. 90, 329 336. https://doi.org/10.1016/j.watres.2015.12.028.

Theophile, T. (Ed.), 2012. Infrared Spectroscopy - Materials Science, Engineering and Technology. InTech.

Wang, J., Li, K., Wei, Y., Cheng, Y., Wei, D., Li, M., 2015. Performance and fate of organics in a pilot MBR NF for treating antibiotic production wastewater with recycling NF concentrate. Chemosphere 121, 92 100. https://doi.org/10.1016/j.chemosphere.2014.11.034.

Wei, X., Wang, Z., Fan, F., Wang, J., Wang, S., 2010. Advanced treatment of a complex pharmaceutical wastewater by nanofiltration: membrane foulant identification and cleaning. Desalination 251, 167 175. https://doi.org/10.1016/j.desal.2009.08.005.

Xiao, K., Xu, Y., Liang, S., Lei, T., Sun, J., Wen, X., Zhang, H., Chen, C., Huang, X., 2014. Engineering application of membrane bioreactor for wastewater treatment in China: current state and future prospect. Front. Environ. Sci. Eng. 8, 805 819. https://doi.org/10.1007/s11783-014-0756-8.

Zydney, A.L., 1997. Stagnant film model for concentration polarization in membrane systems. J. Membr. Sci. 130, 275 281. https://doi.org/10.1016/S0376-7388(97)00006-9.